of the kidney ($P < .0001$). These data suggest that ABCF2 protein may be a candidate marker for clear cell adenocarcinomas of the ovary and the uterine corpus and may be important for the pathogenesis of these diseases.

1. Introduction

Resistance to chemotherapeutic agents is a major obstacle for successful treatment of cancer. The sensitivity to chemotherapy is generally related to pathologic findings, such as histologic type or grade of the tumor, even if they share the same origin. For example, epithelial ovarian cancer can be subdivided into 5 major histologic types (serous, mucinous, endometrioid, clear cell, and poorly differentiated). Among them, clear cell ovarian cancer, which constitutes 5% to 10% of ovarian cancer cases in the Unites States, differs from other histologic types with respect to its clinical characteristics [1,2]. Clear cell ovarian cancer is usually more resistant to systemic chemotherapy than other types and has a worse prognosis [3,4]. We previously reported that ABCF2 protein expression is higher in clear cell type than serous type, and its expression correlates with chemoresponse in patients with clear cell ovarian cancer [5]. In this study, we further examined ABCF2 protein expression in mucinous, endometrioid, and poorly differentiated types of ovarian cancer and compared it with that of the clear cell and serous types.

Clear cell adenocarcinomas have been found to develop in different organs such as the ovary, the uterine corpus, and the kidney, and the prognosis of this cancer is usually poor [3,4.6,7]. In the cancer of uterine corpus, clear cell and serous adenocarcinomas have worse prognosis, compared with that of the endometrioid type, which constitutes 80% of uterine corpus cancer [6]. Clear cell adenocarcinoma of the kidney is thought to be chemoresistant [7,8]. Clear cell adenocarcinoma of the ovary is morphologically similar to clear cell adenocarcinomas developed from the uterine corpus or the kidney. However, both clear cell adenocarcinomas of the ovary and uterine corpus are Mullerian in origin, whereas those developed from the kidney are Wolffian duct in origin [9]. Candidate biomarkers that can be used successfully to differentiate these tumors have not been identified. In this study, we further evaluated whether significant differences in ABCF2 protein expression can be identified in clear cell adenocarcinoma of the ovary, the uterine corpus, and the kidney.

2. Materials and methods

2.1. Clinical samples

A total of 335 epithelial ovarian cancers, 23 clear cell adenocarcinomas of uterine corpus, and 34 clear cell adenocarcinomas of kidney were included in this study. Median age of patients with ovarian cancer is 54 years (range, 22-85 years). In ovarian cancer, histologic types were as follows: 102 serous adenocarcinomas, 50 mucinous adenocarcinomas, 76 clear cell adenocarcinomas, 74 endometrioid adenocarcinomas, and 33 undifferentiated carcinomas. Twenty-two of 76 clear cell cases and 15 of 102 serous cases were previously reported [5]. Median age of patients with clear cell adenocarcinoma of the uterine corpus and the kidney is 62 (range, 48-83) and 65 (range, 30-86) years. The clinical background is shown in Table 1. All patient-derived paraffin sections were collected and archived under protocols approved by the institutional review boards of the parent institutions.

2.2. Immunohistochemistry

Immunolocalization of the ABCF2 protein was performed using a polyclonal anti-ABCF2 antibody generated by injecting the purified full-length ABCF2 fusion protein into

Table 1 Clinical background of each histologic type

	Clinical stage		Histologic grade		
	Stage I + II	Stage III + IV	Well/moderate	Poor	Total
Epithelial ovarian cancer					
Serous	34	68	70	32	102
Mucinous	34	16	48	2	50
Clear cell	47	29	65	11	76
Endometrioid	30	44	44	30	74
Poorly differentiated	4	29	0	33	33
Total					336
Clear cell adenocarcinoma					
Uterine corpus	14	9	–	–	23
Kidney	24	10	–	–	34

Table 2 ABCF2 expression in epithelial ovarian cancer

Parameter	ABCF2 (cytoplasm)			ABCF2 (nuclear)	
	Positive	Negative	*P*	LI (95% CI)	*P*
Age					
<Median	104	64	NS	7.1 (4.9-9.3)	.004
>Median	106	62		13.7 (9.8-17.5)	
FIGO stage					
I + II	100	49	NS	12.2 (8.8-15.5)	NS
III + IV	110	77		9.1 (6.1-12.1)	
Histologic type					
Clear	66	10		21.1 (15.5-26.8)	
Serous	54	48	<.0001	10.2 (5.8-14.6)	.01
Mucinous	23	27	<.0001	4.2 (1.8-6.6)	.0003
Endometrioid	43	31	<.0001	4.7 (1.8-7.6)	<.0001
Undifferentiated	24	10	NS	9.1 (0.04-18.1)	.03
Differentiation grade					
Well/moderate	141	86	NS	11.2 (8.6-13.8)	NS
Poor	69	40		8.8 (4.6-13.1)	

Abbreviations: LI, labeling index; NS, nonsignificant; FIGO, International Federation of Gynecologists and Obstetricians.

the rabbits [5]. In brief, histologic sections (4 μm) were affixed to glass slides, dewaxed, and rehydrated. The sections were then incubated in 3% hydrogen peroxide for 10 minutes at room temperature to quench endogeneous peroxidase activity. The sections were reacted with the ABCF2 antibody (×5000) at 4°C overnight. The peroxidase activity for all proteins was visualized by applying diaminobenzidine chromogen containing 0.05% hydrogen peroxide for 2 to 10 minutes at room temperature. The sections were then counterstained with hematoxylin. The slides were read by 2 independent pathologists who were blinded to the clinical background of the patients. Positive cells were counted for ABCF2 protein in the nuclei by examining at least 1000 tumor cells. Levels of ABCF2 were scored based on the percentage of cells with positive nuclear staining. ABCF2 cytoplasmic staining groups were divided into positive or negative. Slides of epithelial ovarian cancer known to be either positive or negative for ABCF2 expression were used as positive and negative controls, respectively [5].

2.3. Statistical analysis

The relationship between ABCF2 expression and age, clinical stage, and histologic grade were analyzed using *t* test and χ^2 test. Differences of ABCF2 expression in cytoplasm among the histologic groups of ovarian cancer were analyzed by the method of Ryan [10]. Differences of ABCF2 expression in nuclei among the histologic groups of ovarian cancer were examined by 1-way analysis of variance, followed by Tukey-Kramer tests. To determine whether any significant effects could be explained by other variables, a multivariate logistic regression model or multivariate regression model was performed with the following covariates in the model: age in years, clinical stage, histologic type, and histologic grade.

The comparison of ABCF2 expression in nuclei and cytoplasm in clear cell adenocarcinoma of ovary, endometrium, and kidney were evaluated using *t* test and χ^2 test.

3. Results

3.1. ABCF2 expression in ovarian cancer

In all histologic types of ovarian cancer, nuclear ABCF2 expression was lower in the younger age group (less than median age) (7.1 versus 13.7, $P = .004$) (Table 2). However, there was no significant difference in ABCF2 in cytoplasm expression between both groups. There was no significant relationship between clinical stage, histologic grade, and

Fig. 1 A, Positive immunostaining of ABCF2 in clear cell adenocarcinoma of the ovary. B, Negative immunostaining of ABCF2 in clear cell adenocarcinoma of the ovary. C, Positive immunostaining of ABCF2 in serous cystadenocarcinoma. D, Negative immunostaining of ABCF2 in serous cystadenocarcinoma. E, Positive immunostaining of ABCF2 in mucinous cystadenocarcinoma. F, Negative immunostaining of ABCF2 in mucinous cystadenocarcinoma. G, Positive immunostaining of ABCF2 in endometrioid adenocarcinoma. H, Negative immunostaining of ABCF2 in endometrioid adenocarcinoma. I, Positive immunostaining of ABCF2 in undifferentiated adenocarcinoma. J, Negative immunostaining of ABCF2 in undifferentiated adenocarcinoma. K, Immunostaining of ABCF2 in normal ovary. L, Positive immunostaining of ABCF2 in clear cell adenocarcinoma of the uterine corpus. M, Negative immunostaining of ABCF2 in clear cell adenocarcinoma of the uterine corpus. N, Positive immunostaining of ABCF2 in clear cell adenocarcinoma of the kidney. O, Negative immunostaining of ABCF2 in clear cell adenocarcinoma of the kidney.

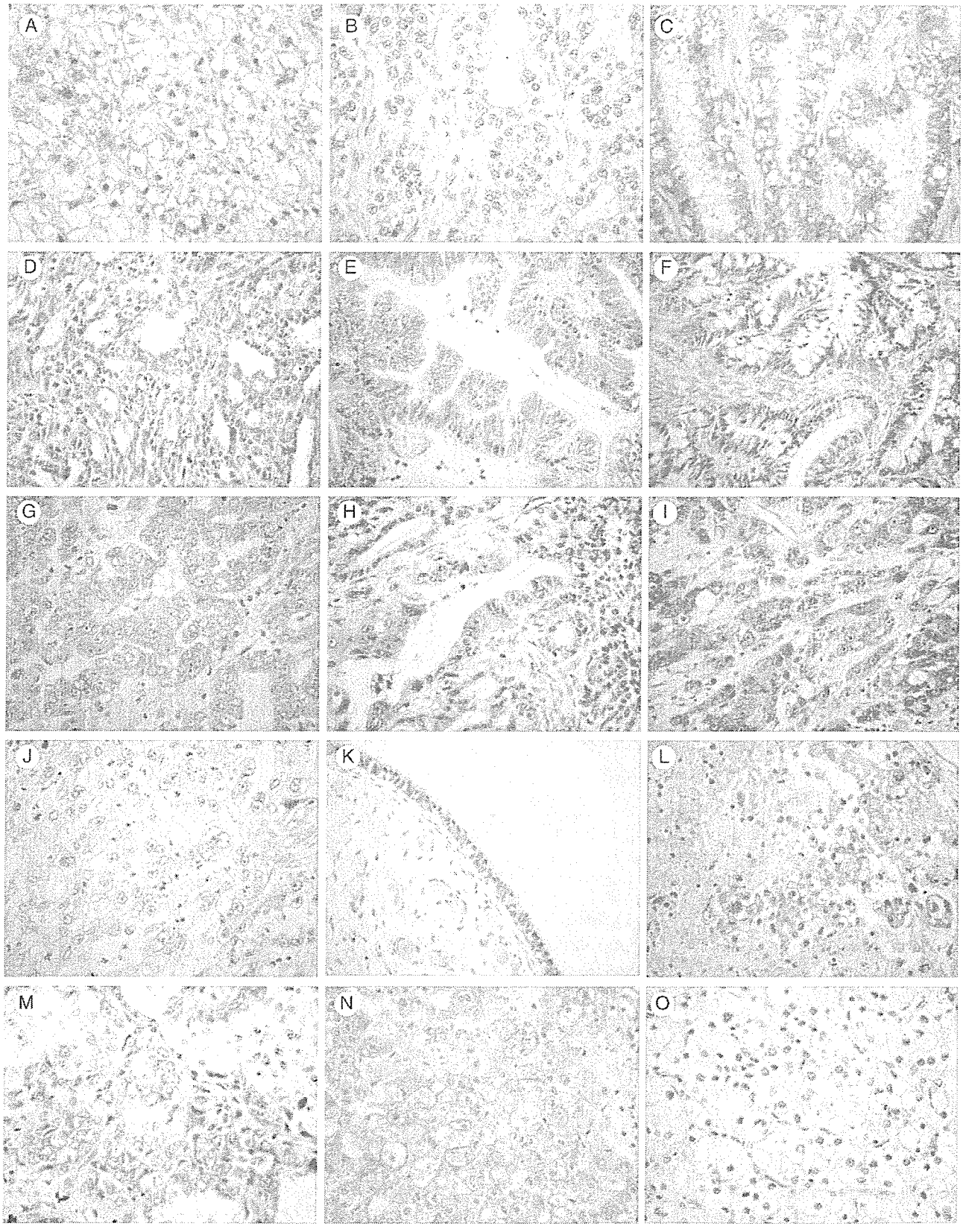
A
B
C
D
E
F
G
H
I
J
K
L
M
N
O

Table 3 Multivariable predictors of ABCF2 expression

Parameter	ABCF2 (cytoplasm)			ABCF2 (nuclear)		
	OR	95% CI	*P*	OR	95% CI	*P*
Age	1.119	0.699-1.791	.639	7.254	2.953-11.556	.001
FIGO stage	0.778	0.477-1.27	.316	−2.035	−6.485 to 2.414	.369
Histologic type	5.557	2.694-11.462	<.0001	13.587	8.345-18.829	<.001
Histologic grade	0.692	0.416-1.152	.157	0.375	−4.388-5.087	.876

NOTE. Age, greater than versus less than median; Stage, III + IV versus I + II; Histologic type, clear cell versus non–clear cell; histologic grade, well/moderate versus poor.

ABCF2 expression in nuclei or cytoplasm (Table 2). Labeling index of ABCF2 expression in nuclei is higher in clear cell adenocarcinoma than in serous, mucinous, endometrioid, and undifferentiated adenocarcinoma (21.1 versus 10.2, 4.2, 4.7, and 9.1; P = .01, .0003, <.0001, and .03, respectively) (Table 2). The frequency of ABCF2 expression in cytoplasm was 86.8%, 52.9%, 46.0%, 58.1%, and 70.6% in clear cell, serous, mucinous, endometrioid, and undifferentiated types, and it is higher in clear cell than in serous, mucinous, and endometrioid adenocarcinoma (P < .0001) (Table 2). Representative images of immunolocalization of ABCF2 in ovarian cancer and normal ovary are shown in Fig. 1A-K. Normal ovarian epithelium was weakly stained.

The multivariate logistic regression model showed that clear cell histology was associated with ABCF2 expression in cytoplasm (odds ratio [OR], 5.557; 95% confidence interval [CI], 2.694-11.462; P < .0001). The multivariate regression model showed that age greater than median age and clear cell histology were associated with ABCF2 expression in nuclei (OR, 7.254; 95% CI, 2.953-11.556; P = .001) (OR, 13.587; 95% CI, 8.345-18.829; P < .001) (Table 3).

3.2. ABCF2 expression in clear cell adenocarcinoma of the ovary, uterine corpus, and the kidney

There were no significant differences in ABCF2 nuclear or cytoplasmic expression between clear cell adenocarcinoma of the ovary and the uterine corpus. However, the cytoplasmic and nuclear ABCF2 expression rate was significantly higher in clear cell adenocarcinoma of the ovary and uterine corpus than in the kidney (86.8% versus 38.2%, P < .0001; 21.1 versus 1.9, P < .0001) (Table 4). ABCF2 expression was not associated with clinical stage in clear cell adenocarcinoma of the ovary, the uterine corpus, and the kidney. Representative images of immunohistochemistry of clear cell adenocarcinoma of uterine corpus and kidney are shown in Fig. 1L-O.

4. Discussion

Clear cell ovarian cancer is a relatively uncommon histologic type of epithelial ovarian cancer, and its molecular basis remains unclear. We previously reported that ABCF2 protein is highly expressed in clear cell type compared with serous-type ovarian cancer, and its expression is related to chemotherapy response [5]. In this study, we further investigate ABCF2 protein expression patterns among 5 histologic types of epithelial ovarian cancer. The results showed that clear cell cancer expressed significantly higher levels of ABCF2 than that of other histologic types. It is particularly interesting that clear cell and endometrioid type of ovarian cancers expressed different levels of ABCF2 in spite that both of them are believed to develop from endometriosis [2]. These findings further support the hypothesis that different histologic types of ovarian cancer have different pathogenetic pathways, and ABCF2 may play different roles in different histologic types of ovarian cancer.

In this study, we found that ABCF2 was expressed in 86.8% of clear cell ovarian cancer. In addition, we showed that ABCF2 was expressed in 89.4% of stage I and II clear cell cancers. These data suggest that ABCF2 may be used as a marker for early detection of the disease. Currently, CA125, a glycoprotein recognized by the monoclonal antibody OC125 [11], is found to be elevated in more than 80% of ovarian cancer, and it is an excellent tumor marker of ovarian cancer [12]. However, CA125 elevation rate is relatively low in clear cell ovarian cancer or in early stage of ovarian cancer [13,14]. Because clear cell type of ovarian cancer is usually more resistant to systemic chemotherapy than other histologic types and has a worse prognosis [3,4], early diagnosis is essential especially for clear cell ovarian cancer. Finding new tumor markers for this type of ovarian tumor is particularly important.

Clear cell adenocarcinoma can arise from the ovary, the uterine corpus, and the kidney. These 3 types of clear cell adenocarcinomas are morphologically indistinguishable from one another. It has been shown that clear cell adenocarcinomas of both ovary and kidney are chemoresistant [3,4,7,8]. Molecular markers that can be used to differentiate clear cell cancers in different organs have not been identified. In addition, the mechanism of chemoresistance of kidney clear cell adenocarcinoma may differ from that in clear cell adenocarcinoma of ovary or uterine corpus. The differential expression patterns may be explained by the fact that both clear cell adenocarcinoma of the ovary and uterine corpus are Mullerian in origin, in

Table 4 ABCF2 expression in clear cell adenocarcinoma of each site

	Cytoplasmic staining	*P*	Nuclear staining	*P*
Ovary	86.8% (66/76)		21.1	
Uterine corpus	91.3% (21/23)	ns	11.5	ns
Kidney	38.2% (13/34)	<.0001	1.9	<.0001

contrast to clear cell adenocarcinoma of the kidney, which is Wolffian duct in origin [8].

In conclusion, our findings suggest that ABCF2 protein may be used as a biomarker to detect clear cell ovarian cancer at early stages and may be important for the pathogenesis of clear cell cancers of Mullerian origin.

Acknowledgment

The authors thank Dr Naoki Kawamura of Osaka City General Hospital for his critical review of the manuscript and Asami Nagata and Nozomi Tsuji for their technical assistance.

References

[1] Scully RE, Young RH, Clement PB. Tumors of the ovary, maldeveloped gonads, fallopian tube, and broad ligament. Atlas of Tumor Pathology. 3rd series, Fascicle 23. Washington (DC): Armed Forces Institute of Pathology; 1998.

[2] Russel P. Surface epithelial-stroma tumors of the ovary. In: Kurman RJ, editor. Blaustein's pathology of the female genital tract. 4th ed. New York: Springer-Verlag; 1994. p. 705-82.

[3] Goff BA, Sainz de la Cuesta R, Muntz HG, et al. Clear cell carcinoma of the ovary: a distinct histologic type with poor prognosis and resistance to platinum-based chemotherapy in stage 3 disease. Gynecol Oncol 1996;60:412-7.

[4] Behbakht K, Randall TC, Benjamin I, Morgan MA, King S, Rubin SC. Clinical characteristics of clear cell carcinoma of the ovary. Gynecol Oncol 1998;70:255-8.

[5] Tsuda H, Ito YM, Ohashi Y, et al. Identification of overexpression and amplification of ABCF2 in clear cell ovarian adenocarcinomas by cDNA microarray analyses. Clin Cancer Res 2005;11:6880-8.

[6] Abeler VM, Kjorstad KE, Berle E. Carcinoma of the endometrium in Norway: a histopathological and prognostic survey of a total population. Int J Gynecol Cancer 1992;2:9-22.

[7] Yagoda A. Phase II cytotoxic chemotherapy trials in RCC: 1983-1988. Prog Clin Biol Res 1990;350:227-41.

[8] Bukowski RM. Natural history and therapy of metastatic renal cell carcinoma. Cancer 1997;80:1198-220.

[9] Matias-Guiu X, Lerma E, Part J. Clear cell tumors of the female genital tract. Semin Diagn Pathol 1997;14:233.

[10] Ryan TA. Significance tests for multiple comparison of proportions, variances, and other statistics. Psychol Bull 1960;57:318-28.

[11] Bast RC, Feeney M, Lazarus H, Nadler LM, Colvin RB, Knapp RC. Reactivity of a monoclonal antibody with human ovarian carcinoma. J Clin Invest 1981;68:1331-7.

[12] Bast Jr RC, Klug TL, St John E, et al. A radioimmunoassay using a monoclonal antibody to monitor the course of epithelial ovarian cancer. N Engl J Med 1983;309:883-7.

[13] Jacobs I, Bast Jr RC. The CA125 tumour-associated antigen: a review of the literature. Hum Reprod 1989;4:1-12.

[14] Vergote IB, Bormer OP, Abeler VM. Evaluation of serum CA125 levels in the monitoring of ovarian cancer. Am J Obstet Gynecol 1987;157:88-92.

Int J Gynecol Cancer 2006, **16**, 979–985

ORIGINAL ARTICLES

Genetic variation in *ABCB1* influences paclitaxel pharmacokinetics in Japanese patients with ovarian cancer

H. YAMAGUCHI*†, T. HISHINUMA*†, N. ENDO*, H. TSUKAMOTO*, Y. KISHIKAWA†, M. SATO†, Y. MURAI†, M. HIRATSUKA‡, K. ITO§, C. OKAMURA§, N. YAEGASHI§, N. SUZUKI*†, Y. TOMIOKA*† & J. GOTO*†

**Division of Clinical Pharmacy, Graduate School of Pharmaceutical Sciences, Tohoku University, Sendai, Japan; †Department of Pharmaceutical Sciences, Tohoku University Hospital, Sendai, Japan; ‡Department of Clinical Pharmaceutics, Tohoku Pharmaceutical University, Sendai, Japan; and §Department of Obstetrics and Gynecology, Graduate School of Medicine, Tohoku University, Sendai, Japan*

Abstract. Yamaguchi H, Hishinuma T, Endo N, Tsukamoto H, Kishikawa Y, Sato M, Murai Y, Hiratsuka M, Ito K, Okamura C, Yaegashi N, Suzuki N, Tomioka Y, Goto J. Genetic variation in *ABCB1* influences paclitaxel pharmacokinetics in Japanese patients with ovarian cancer. *Int J Gynecol Cancer* 2006;**16**:979–985.

Paclitaxel, an antineoplastic agent used for the treatment of ovarian cancer, is metabolized by cytochrome P450 (CYP)3A4 and CYP2C8 and is excreted from cells by ATP-binding cassette (ABCB1) (multi-drug resistance [MDR1], P-glycoprotein). Expression of these proteins is regulated by pregnane X receptor (PXR). Although there are common genetic polymorphisms in the genes encoding these proteins, their effect on the clinical efficacy of paclitaxel is unclear. We therefore examined the relationship of the paclitaxel pharmacokinetics in 13 patients with ovarian cancer to polymorphisms in *CYP2C8*, *CYP3A5*, *ABCB1*, and *PXR*. We found high interindividual variability in the plasma concentrations of two metabolites, 6α-hydroxypaclitaxel and *p*-3′-hydroxypaclitaxel. All the patients were genotyped as *CYP2C8*1/*1*. Neither the *CYP3A5* A6986G (*CYP3A5*3*) nor the *PXR* C-25385T alleles were associated with altered plasma concentrations of paclitaxel and its metabolites. *ABCB1* T-129C, T1236C, and G2677(A,T), however, was associated with lower area under the plasma concentration–time curve (AUC) of paclitaxel. We also observed a significant correlation between the AUC ($r = -0.721$) or the total clearance of paclitaxel (CL_{tot}) ($r = 0.673$) and the *ABCB1* mutant allele dosage in each patient. Taken together, our findings suggest that interindividual variability in paclitaxel pharmacokinetics could be predicted by *ABCB1* genotyping.

KEYWORDS: ABCB1, genetic polymorphisms, ovarian cancer, paclitaxel pharmacokinetics.

Paclitaxel has a significant clinical activity against multiple cancers, including ovarian, breast, and lung tumors[1]. The stabilization of microtubules by paclitaxel results in cell cycle arrest. Although highly effective, earlier studies have demonstrated a high degree of interindividual variability in resulting plasma paclitaxel concentrations[2]. Paclitaxel therapy is typically associated with a number of toxic side effects, most commonly neutropenia, peripheral neuropathy, nausea, and vomiting[3]. Previous studies reported a correlation between toxicity and paclitaxel plasma

Address correspondence and reprint requests to: Junichi Goto, PhD, Department of Pharmaceutical Sciences, Tohoku University Hospital, 1-1 Seiryo-machi, Aoba-ku, Sendai 980-8574, Japan. Email: jun-goto@pharm.med.tohoku.ac.jp

H. Tsukamoto is presently at Institute for Environmental and Gender Specific Medicine, Graduate School of Medicine, Juntendo University, Urayasu, Japan; and N. Suzuki is presently at Department of Clinical Pharmacy, Faculty of Pharmaceutical Sciences, Josai International University, Togane, Japan.

concentrations when the drug was given at lower doses or during shorter infusion times[4,5]. The mechanisms underlying the interindividual variabilities of drug toxicity, however, remain poorly understood.

Systemic elimination of paclitaxel occurs primarily via hepatic metabolism and biliary excretion[6]. Formation of the major metabolite, 6α-hydroxypaclitaxel, is catalyzed by cytochrome P450 (CYP) 2C8[7,8], while the other metabolite, *p*-3′-hydroxypaclitaxel, is formed by the action of CYP3A4[7,9]. The dihydroxylated metabolite is thought to result from the stepwise hydroxylation of the two previously described sites. Although CYP3A5 is not responsible for paclitaxel hydroxylation[9], Kuehl *et al.*[10] reported that this protein can account for greater than 50% of the total CYP3A in people who express this allele. Therefore, CYP3A5 polymorphisms may contribute to the observed interindividual differences in paclitaxel clearance. Paclitaxel is also a substrate of the drug efflux transporter ABCB1 (MDR1, P-glycoprotein)[11,12], which is normally expressed in the billiary tract, intestine, renal tubules, and brain. ABCB1 plays a principal role in maintenance of the absorption barrier and elimination of xenobiotics, such as paclitaxel, from the body[13]. The pregnane X receptor (PXR) is a xenobiotic-regulated transcription factor that coordinately activates transcription of *CYP2C8* and *CYP3A4* in the liver and *ABCB1* in the intestine[14]. Thus, PXR is a master regulator of drug clearance; any functional variants will likely have widespread effects on paclitaxel pharmacokinetics. Although common genetic polymorphisms in these genes could influence paclitaxel efficacy, the relationship of these alleles to paclitaxel pharmacokinetics has not been fully evaluated.

In this study, we examined the pharmacokinetics of paclitaxel and metabolites formed by CYP2C8 or CYP3A4 and known functional polymorphisms of *CYP2C8*, *CYP3A5*, *ABCB1*, and *PXR*. In Japanese patients undergoing paclitaxel and carboplatin combination therapy for diagnosed ovarian cancer, we then correlated these genotypes with paclitaxel pharmacokinetics.

Materials and methods

Patients

Paclitaxel pharmacokinetics was studied in 13 patients with newly diagnosed ovarian cancer undergoing first-line chemotherapy. The mean age of the patients was 53 years, ranging from 31 to 73 years (Table 1). All clinical protocols, including blood sampling for pharmacokinetic and pharmacogenetic analyses, were approved by the ethical committee of Tohoku University School of Medicine. Genotyping was performed in above-mentioned patients and unrelated healthy Japanese volunteers. All subjects provided their written informed consent for participation in the sampling protocol.

Table 1. Patient characteristics

Characteristic	Patients
Age, mean ± SD (years)	53 ± 12
Body surface area, mean ± SD (m^2)	1.45 ± 0.09
Sampling time points after paclitaxel infusion	
1, 3, 6, and 19 h	3
3, 6, 9, and 19 h	1
3, 4, 6, 9, and 19 h	3
1, 2, 3, 4, 6, 9, and 19 h	6

Genotyping

Genomic DNA was extracted from peripheral blood cells, treated with K_2EDTA as an anticoagulant, using a GFX Genomic Blood DNA Purification Kit (Amersham Pharmacia Biotech, Buckinghamshire, UK), according to the manufacturer's recommendations. *CYP2C8* A805T (*CYP2C8*2*), G416A/A1196G (*CYP2C8*3*), and C792G (*CYP2C8*4*), and *ABCB1* T-129C, T1236C, G2677(A,T), and C3435T were genotyped by polymerase chain reaction (PCR)–restriction enzyme fragment length polymorphism as previously described with minor modification[15–17]. The *CYP2C8* 475A deletion (*CYP2C8*5*) and the C1210G, *CYP3A5* A6986G (*CYP3A5*3*), and *PXR* C-25385T alleles were genotyped by allele-specific real-time PCR with SYBR Green using an ABI PRISM 7700 sequence detection system (Applied Biosystems, Foster City, CA) as described[18]. Briefly, in a 20 μL reaction mixture containing 2× SYBR Green PCR Master Mix (QIAGEN, Valencia, CA), 0.4 μM forward and reverse primers were used to amplify the specified sequences from 20 to 100 ng genomic DNA. PCR products were detected following amplification by 1 cycle of 95°C for 15 min and 35 cycles of 95°C for 30 sec, 60°C for 30 sec, and 72°C for 30 sec. The PCR primers used are shown in Table 2.

Pharmacokinetics studies

Paclitaxel was administered intravenously over a 3-h infusion period at a dose of approximately 175 mg/m^2 (163–194 mg/m^2). Plasma samples were obtained at four to seven time points within 1–19 h after the start of the infusion. After centrifugation, plasma samples were stored at –80°C until analysis. We measured the concentrations of paclitaxel, 6α-hydroxypaclitaxel, and

Table 2. Summary of primer pair sequences (5′–3′) used in allele-specific real-time PCR assays with SYBR Green

CYP2C8	
475A deletion	
(*CYP2C8*5*)	
WP	GTCACCCACCCTTGGTTTTTC
MP	GTCACCCACCCTTGGTTTTC
CP	TGAATTCTCCCAGTTTCTGCCC
C1210G	
WP	GCTACATGATGACAAAGAATTTCCTAATC
MP	GCTACATGATGACAAAGAATTTCCTAATG
CP	CCTTTAAATACAAATGGAAACGAG
CYP3A5	
A6986G	
(*CYP3A5*3*)	
WP	TCTCTTTAAAGAGCTCTTTTGTCTTTCGA
MP	TCTCTTTAAAGAGCTCTTTTGTCTTTCGG
CP	CAACCTTAGGTTCTAGTTCATTAGGGTG
PXR	
C-25385T	
WP	CATTTTTTGGCAATCCCAGGTTC
MP	CATTTTTTGGCAATCCCAGGTTT
CP	AGATGCTTTATGGCAGGTGAGGG

WP, wild-type primer; MP, mutant primer; CP, common primer.

p-3′-hydroxypaclitaxel in all patients by reverse-phase high-performance liquid chromatography as described[19]. Briefly, cephalomannine was added to each plasma sample as an internal standard. Paclitaxel, 6α-hydroxypaclitaxel, and *p*-3′-hydroxypaclitaxel were extracted using a 1-mL Bond Elut C18 cartridge (Varian, Harbor City, CA). The high-performance liquid chromatography system consisted of a Nanospace SI-1 (Shiseido, Tokyo, Japan) equipped with an ultraviolet ray detector at 230 nm. Chromatography was performed on a C18 Capcell Pak UG120 column (Shiseido; 1.5 × 150 mm, 5 μm) at 40°C using isocratic elution in acetonitrile–20 mM ammonium acetate (38:62, vol/vol, pH 5.0) at a flow rate of 100 μL/min. The pharmacokinetic parameters, including the area under the plasma concentration–time curve (AUC), mean residence time, volume of distribution at steady state (V_{dss}), and total clearance (CL_{tot}), were calculated by moment analysis as described[20].

Statistical analysis

All pharmacokinetic data are presented as mean ± SD. To relate the pharmacokinetic parameters to each polymorphism, the Mann–Whitney *U* test was used for two group comparisons. When more than two groups were compared, the Kruskal–Wallis test was used. The correlation between the pharmacokinetic parameters and the number of *ABCB1* mutant alleles in our subjects was estimated by the Spearman rank correlation. *P* values < 0.05 were considered to be significant.

Results

Genotyping

There is little information concerning the frequency of *CYP2C8* and *PXR* polymorphisms in the Japanese population. In a preliminary study, we screened for previously described polymorphisms of *CYP2C8* and *PXR* in DNA samples from 210 and 90 Japanese individuals, respectively. We found only one subject genotyped as a heterozygote of *CYP2C8*3*, giving an allele frequency of 0.0024. No other polymorphisms in the *CYP2C8* gene were observed. The genotype frequencies of *PXR* were 0.511 for wild type, 0.456 for the C-25385T heterozygote, and 0.033 for homozygous C-25385T mutants. Therefore, the mutant allele frequency was 0.261, which is lower

Table 3. *CYP2C8*, *CYP3A5*, *ABCB1*, and *PXR* genotypes in 13 patients[a]

		CYP3A5	*ABCB1*				*PXR*
Patient number	*CYP2C8*	A6986G	T-129C	T1236C	G2677 (A,T)	C3435T	C-25385T
1	*1/*1	A/G	T/T	T/T	G/T	C/T	C/C
2	*1/*1	A/G	T/T	T/C	A/T	C/C	C/C
3	*1/*1	G/G	T/T	T/C	G/G	C/T	C/C
4	*1/*1	A/G	T/T	T/T	T/T	T/T	C/T
5	*1/*1	A/A	T/T	T/T	G/T	C/T	T/T
6	*1/*1	A/G	T/T	T/T	G/G	C/C	C/C
7	*1/*1	G/G	T/T	T/C	G/G	C/C	C/C
8	*1/*1	G/G	T/T	T/T	G/T	C/T	C/T
9	*1/*1	A/G	T/T	T/T	G/T	C/T	C/C
10	*1/*1	G/G	T/T	T/T	G/T	C/T	C/C
11	*1/*1	A/G	T/T	T/C	G/T	C/C	C/T
12	*1/*1	G/G	T/C	C/C	A/A	C/C	C/T
13	*1/*1	G/G	T/T	T/C	G/T	C/T	C/C

[a]The most common (wild-type) *CYP2C8* allele was *CYP2C8*1*.

than the frequencies of 0.39 and 0.32 observed for Caucasian and African American populations, respectively[21]. These results correlated well with the expected genotype distributions of the examined genes calculated by the Hardy–Weinberg equation.

We also examined the *CYP2C8*, *CYP3A5*, *ABCB1*, and *PXR* genotypes in 13 Japanese patients (Table 3). None of the 13 patients genotyped possessed the *CYP2C8*2*, *CYP2C8*3*, *CYP2C8*4*, *CYP2C8*5*, or C1210G alleles; all were genotyped as *CYP2C8*1/*1*.

Pharmacokinetics of paclitaxel

Plasma concentration–time curves of paclitaxel, 6α-hydroxypaclitaxel, and *p*-3′-hydroxypaclitaxel are shown in Figure 1; the pharmacokinetic parameters are summarized in Table 4. Interindividual variabilities between the lowest and the highest values diverged to 3.4-, 2.6-, 2.1-, and 2.3-fold for paclitaxel maximum drug concentration (C_{max}), AUC, V_{dss}, and CL_{tot}, respectively. The AUC ratios were also highly variable, with 12.5-, 5-, and 8-fold differences between the lowest and the highest values for 6α-hydroxypaclitaxel/paclitaxel (×100), *p*-3′-hydroxypaclitaxel/paclitaxel (×100), and 6α-hydroxypaclitaxel/*p*-3′-hydroxypaclitaxel, respectively. The AUC ratio of 6α-hydroxypaclitaxel to *p*-3′-hydroxypaclitaxel in patients 4, 10, and 11 was approximately 1, while this value in the remaining patients was below 1. These results suggest that the metabolic activity of CYP2C8 is similar to or slightly lower than that of CYP3A4 against paclitaxel in Japanese subjects.

Correlation of genotype and pharmacokinetic parameters

As none of the examined patients possessed *CYP2C8* variant alleles, we could not examine the correlation between paclitaxel pharmacokinetic parameters and *CYP2C8* polymorphisms.

For the *CYP3A5*1/*1*, **1/*3*, and **3/*3* genotypes ($n = 1$, 6, and 6), mean paclitaxel AUC were 12.0, 9.78 ± 1.43, and 10.5 ± 3.41 μg·h/mL and the *p*-3′-hydroxypaclitaxel/paclitaxel (×100) AUC ratios were 6.06, 5.21 ± 3.37, and 6.39 ± 3.20, respectively. There were no obvious trends in either the mean paclitaxel AUC or the *p*-3′-hydroxypaclitaxel/paclitaxel AUC ratio that would suggest an effect of *CYP3A5*3* genotype on these parameters.

The patient heterozygous for the *ABCB1* T-129C allele exhibited a lower paclitaxel AUC than the wild-type homozygotes (5.73 versus 10.7 ± 2.14 μg·h/mL; $n = 1$ versus 12). Although the differences were not statistically significant, *ABCB1* T1236C tended to be associated with lower paclitaxel AUC (11.4 ± 2.32, 9.62 ± 1.48, and 5.73 μg·h/mL for 1236T/T, T/C, and C/C genotypes [$n = 7$, 5, and 1], respectively). Individuals homozygous for the *ABCB1*

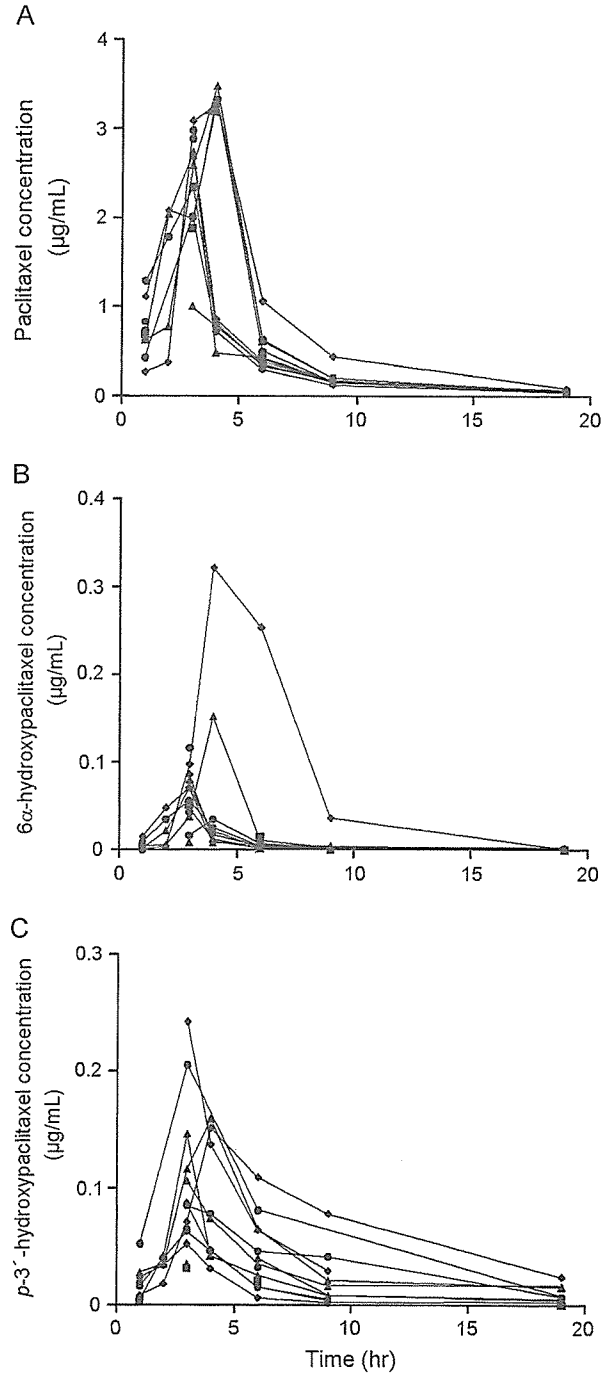

Figure 1. Plasma concentration–time curves for A) paclitaxel, B) 6α-hydroxypaclitaxel, and C) *p*-3′-hydroxypaclitaxel. Paclitaxel was administered intravenously in a 3-h infusion at a dose of approximately 175 mg/m^2. Plasma samples were obtained from 1–19 h after the start of the infusion in four to seven time points, as shown in Table 1.

Table 4. Summary of pharmacokinetic parameters ($n = 13$)

Parameter	Mean ± SD	Range
Paclitaxel		
C_{max} (μg/mL)	2.59 ± 0.67	1.00–3.46
AUC (μg·h/mL)	10.3 ± 2.47	5.7–15.0
MRT (h)	5.2 ± 0.7	4.3–6.2
V_{dss} (L/m^2)	96 ± 34	61–190
CL_{tot} (mL/min/m^2)	303 ± 767	215–499
6α-hydroxypaclitaxel		
AUC (μg·h/mL)	0.29 ± 0.36	0.09–1.47
p-3′-hydroxypaclitaxel		
AUC (μg·h/mL)	0.63 ± 0.42	0.18–1.42
AUC ratios		
6α-hydroxypaclitaxel/ *p*-3′-hydroxypaclitaxel	0.51 ± 0.33	0.13–1.03
6α-hydroxypaclitaxel/ paclitaxel	2.55 ± 2.25	0.78–9.80
p-3′-hydroxypaclitaxel/ paclitaxel	5.8 ± 3.1	2.2–10.9

MRT, mean residence time.

G2677(A,T) mutant allele had lower levels of paclitaxel AUC (10.9 ± 2.38, 11.1 ± 2.21, 5.73, 8.26, and 9.14 μg·h/mL for the 2677G/G, G/T, A/A, T/T, and A/T genotypes ([$n = 3$, 7, 1, 1, and 1], respectively). In contrast, there was no difference in the paclitaxel AUC values between the different *ABCB1* C3435T genotypes (9.79 ± 2.73, 10.9 ± 2.42, and 8.26 μg·h/mL for 3435C/C, C/T, and T/T genotypes [$n = 5$, 7, and 1], respectively).

As *ABCB1* T-129C, T1236C, and G2677(A,T) were associated with lower paclitaxel AUC (Fig. 2), we examined the relationships between total *ABCB1* mutant allele numbers and either paclitaxel AUC or CL_{tot} in 13 patients. We observed a significant correlation between paclitaxel AUC ($r = -0.721$, $P < 0.05$) and CL_{tot} ($r = 0.673$, $P < 0.05$) with *ABCB1* mutant allele dosage.

Mean paclitaxel AUC were 10.7 ± 2.30, 9.07 ± 2.95, and 12.0 μg·h/mL for *PXR* -25385C/C, C/T, and T/T ($n = 8$, 4, and 1), respectively. We also determined the 6α-hydroxypaclitaxel/paclitaxel (×100) AUC ratios (3.09 ± 2.75, 1.93 ± 0.56, and 0.78) and the *p*-3′-hydroxypaclitaxel/paclitaxel (×100) AUC ratios (6.92 ± 3.27, 3.56 ± 1.56, and 6.06) for the *PXR*-25385C/C, C/T, and T/T genotypes, respectively. There were no obvious trends in any of these parameters for the *PXR* C-25385T genotypes.

Discussion

This study sought to evaluate the effect of genetic polymorphisms within the coding sequences of proteins involved in paclitaxel elimination to the interindividual differences in paclitaxel exposure. As we observed significant interindividual variability in paclitaxel pharmacokinetics, we explored the reasons underlying this variability.

*CYP2C8*2*, *CYP2C8*3*, *CYP2C8*4*, and C1210G exhibit decreased activity against paclitaxel 6α-hydroxylase *in vitro*[15,16,22,23]. In contrast, *CYP2C8*3* was associated with reduced plasma concentrations of the CYP2C8 substrate repaglinide *in vivo*[24]. The *CYP2C8*5* mutation would be expected to cause several significant amino acid alterations and an early stop codon (http://www.imm.ki.se/CYPalleles/). Although these polymorphisms are expected to affect paclitaxel metabolism, we could not directly examine their influences on paclitaxel metabolism as no *CYP2C8* mutant alleles were detected in any of our patients. This result is consistent with another study reporting these polymorphisms to be rare in the Japanese population[22]. Thus, pharmacokinetic abnormalities in paclitaxel metabolized resulting from *CYP2C8* polymorphisms are likely rare in the Japanese.

The *CYP3A5*3* allele leads to alternative splicing that results in a truncated protein product. This is the most common cause of loss of hepatic CYP3A5 expression[10]. *CYP3A5*3*, which is common in Japanese, may account for the wide variation observed in overall CYP3A activity[25]. In our study, however, paclitaxel metabolism was not affected by the presence of

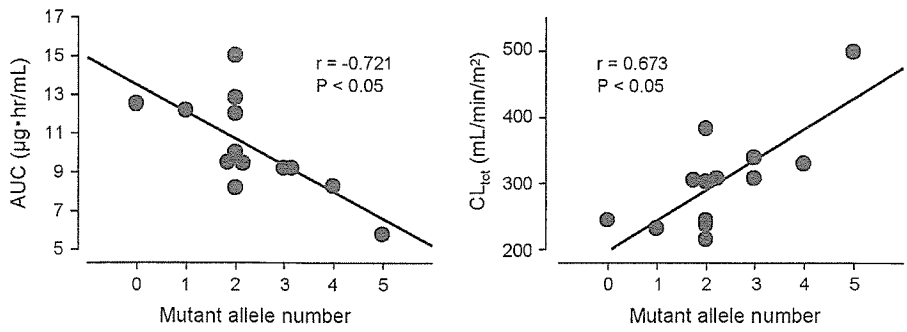

Figure 2. Correlations between paclitaxel AUC and *ABCB1* mutant allele dosage A) and between paclitaxel CL_{tot} and *ABCB1* mutant allele dosage B) in 13 patients treated with a 3-h infusion of paclitaxel. Correlations were analyzed by the Spearman rank order correlation coefficient.

the *CYP3A5*3* allele. This finding is consistent with previous reports, demonstrating that paclitaxel is a substrate for CYP3A4 but not for CYP3A5.

Increasing numbers of reports have correlated *ABCB1* genotype and phenotype with individual variations in drug efficacy. The *ABCB1* T-129C allele affects placental ABCB1 expression[17]. *ABCB1* T1236C is associated with significantly increased exposure to irinotecan and the active metabolite SN-38[26]. The *ABCB1* G2677(A,T) allele exhibits altered ABCB1 function in humans, evidenced by studies using the drug fexofenadine as a probe[27]. *ABCB1* C3435T also influences ABCB1 expression and function[28]. In this study, we demonstrated that patients with the *ABCB1* T-129C, 1236C, and 2677(A,T) alleles displayed lower paclitaxel AUC than subjects with the wild-type allele. We also observed significant correlations between both paclitaxel AUC and CL_{tot} with *ABCB1* mutant allele dosage. These results suggest that *ABCB1* polymorphisms are associated with increased clearance and decreased AUC of paclitaxel. *ABCB1* mutant alleles may be associated with higher membrane transport activity, resulting in increased clearance of paclitaxel by either increased billiary excretion or reduced enterohepatic reabsorption from the gut. Nakajima *et al.*[29] recently reported that ovarian cancer patients possessing the *ABCB1* 3435T allele had higher AUC of *p*-3′-hydroxypaclitaxel compared with those possessing the 3435C allele. They discussed that *p*-3′-hydroxypaclitaxel might be a substrate for ABCB1 with higher affinity rather than paclitaxel. Although we could not get same results (data not shown), it might be due to the different concomitant medication. The *ABCB1* phenotype has a powerful influence on both paclitaxel responses and overall survival[30], suggesting that *ABCB1* single nucleotide polymorphisms (SNPs) may also have influence on patients responses and survival following paclitaxel treatment.

Several SNPs within the PXR promoter correlated with either enhanced or reduced expression of target genes[21]. Of these SNPs, the mutation in the *PXR* C-25385T allele lies within the consensus elements for nuclear factor–kappa B and interferon stimulated gene factor–3 binding. This mutation is the most frequent SNP in Caucasians and African Americans, suggesting that this SNP may also affect paclitaxel metabolism and excretion mediated by CYP2C8, CYP3A4, and ABCB1 in Japanese patients. Our correlational study, however, demonstrates that *PXR* C-25385T did not alter paclitaxel clearance. It will be important to confirm this result and other PXR phenotypic associations in an expanded patient population.

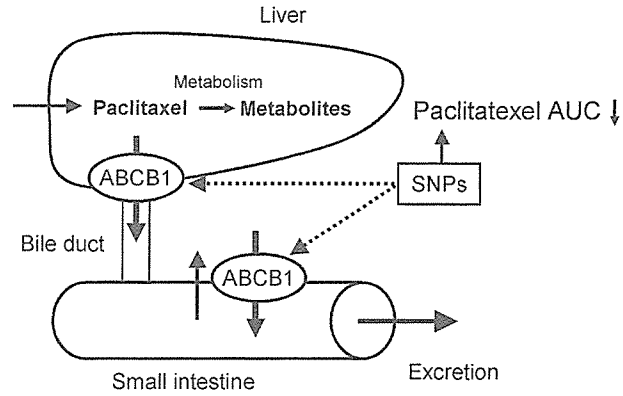

Figure 3. Scheme of proposed effect of *ABCB1* SNPs on paclitaxel disposition.

In conclusion, it may be possible to predict paclitaxel pharmacokinetics by *ABCB1* genotyping (Fig. 3). Although the *ABCB1* polymorphisms analyzed in this study cannot completely account for the differences in paclitaxel pharmacokinetics observed among patients, ABCB1 genotyping may contribute to the achievement of individualized treatment strategies with paclitaxel. Larger comprehensive studies examining the correlations between paclitaxel pharmacokinetics and genetic polymorphisms will be necessary to predict and adjust paclitaxel treatment regimens.

Acknowledgment

This research was supported by a grant from the Ministry of Education, Culture, Sports, Science and Technology and by a research grant from the Uehara Memorial Foundation.

References

1 Rowinsky EK. The development and clinical utility of the taxane class of antimicrotubule chemotherapy agents. *Annu Rev Med* 1997; **48**:353–74.
2 Wiernik PH, Schwartz EL, Strauman JJ, Dutcher JP, Lipton RB, Paietta E. Phase I clinical and pharmacokinetic study of taxol. *Cancer Res* 1987;**47**:2486–93.
3 Brown T, Havlin K, Weiss G *et al.* A phase I trial of taxol given by a 6-hour intravenous infusion. *J Clin Oncol* 1991;**9**:1261–7.
4 Grem JL, Tutsch KD, Simon KJ *et al.* Phase I study of taxol administered as a short i.v. infusion daily for 5 days. *Cancer Treat Rep* 1987;**71**:1179–84.
5 Longnecker SM, Donehower RC, Cates AE *et al.* High-performance liquid chromatographic assay for taxol in human plasma and urine and pharmacokinetics in a phase I trial. *Cancer Treat Rep* 1987;**71**: 53–9.
6 Walle T, Walle UK, Kumar GN, Bhalla KN. Taxol metabolism and disposition in cancer patients. *Drug Metab Dispos* 1995;**23**:506–12.
7 Cresteil T, Monsarrat B, Alvinerie P, Treluyer JM, Vieira I, Wright M. Taxol metabolism by human liver microsomes: identification of cytochrome P450 isozymes involved in its biotransformation. *Cancer Res* 1994;**54**:386–92.

8 Rahman A, Korzekwa KR, Grogan J, Gonzalez FJ, Harris JW. Selective biotransformation of taxol to 6 alpha-hydroxytaxol by human cytochrome P450 2C8. *Cancer Res* 1994;**54:**5543–6.
9 Harris JW, Rahman A, Kim BR, Guengerich FP, Collins JM. Metabolism of taxol by human hepatic microsomes and liver slices: participation of cytochrome P450 3A4 and an unknown P450 enzyme. *Cancer Res* 1994;**54:**4026–35.
10 Kuehl P, Zhang J, Lin Y *et al.* Sequence diversity in CYP3A promoters and characterization of the genetic basis of polymorphic CYP3A5 expression. *Nat Genet* 2001;**27:**383–91.
11 Bradley G, Ling V. P-glycoprotein, multidrug resistance and tumor progression. *Cancer Metastasis Rev* 1994;**13:**223–33.
12 Gottesman MM, Pastan I. Biochemistry of multidrug resistance mediated by the multidrug transporter. *Annu Rev Biochem* 1993;**62:**385–427.
13 Thiebaut F, Tsuruo T, Hamada H, Gottesman MM, Pastan I, Willingham MC. Cellular localization of the multidrug-resistance gene product P-glycoprotein in normal human tissues. *Proc Natl Acad Sci U S A* 1987;**84:**7735–8.
14 Xie W, Evans RM. Orphan nuclear receptors: the exotics of xenobiotics. *J Biol Chem* 2001;**276:**37739–42.
15 Bahadur N, Leathart JB, Mutch E *et al.* CYP2C8 polymorphisms in Caucasians and their relationship with paclitaxel 6alpha-hydroxylase activity in human liver microsomes. *Biochem Pharmacol* 2002; **64:**1579–89.
16 Dai D, Zeldin DC, Blaisdell JA *et al.* Polymorphisms in human CYP2C8 decrease metabolism of the anticancer drug paclitaxel and arachidonic acid. *Pharmacogenetics* 2001;**11:**597–607.
17 Tanabe M, Ieiri I, Nagata N *et al.* Expression of P-glycoprotein in human placenta: relation to genetic polymorphism of the multidrug resistance (MDR)-1 gene. *J Pharmacol Exp Ther* 2001;**297:**1137–43.
18 Hiratsuka M, Agatsuma Y, Mizugaki M. Rapid detection of CYP2C9*3 alleles by real-time fluorescence PCR based on SYBR Green. *Mol Genet Metab* 1999;**68:**357–62.
19 Jamis-Dow CA, Klecker RW, Sarosy G, Reed E, Collins JM. Steady-state plasma concentrations and effects of taxol for a 250 mg/m2 dose in combination with granulocyte-colony stimulating factor in patients with ovarian cancer. *Cancer Chemother Pharmacol* 1993;**33:** 48–52.
20 Yamaoka K, Nakagawa T, Uno T. Statistical moments in pharmacokinetics. *J Pharmacokinet Biopharm* 1978;**6:**547–58.
21 Zhang J, Kuehl P, Green ED *et al.* The human pregnane X receptor: genomic structure and identification and functional characterization of natural allelic variants. *Pharmacogenetics* 2001;**11:**555–72.
22 Nakajima M, Fujiki Y, Noda K *et al.* Genetic polymorphisms of CYP2C8 in Japanese population. *Drug Metab Dispos* 2003;**31:** 687–90.
23 Soyama A, Saito Y, Hanioka N *et al.* Non-synonymous single nucleotide alterations found in the CYP2C8 gene result in reduced in vitro paclitaxel metabolism. *Biol Pharm Bull* 2001;**24:**1427–30.
24 Niemi M, Leathart JB, Neuvonen M, Backman JT, Daly AK, Neuvonen PJ. Polymorphism in CYP2C8 is associated with reduced plasma concentrations of repaglinide. *Clin Pharmacol Ther* 2003;**74:**380–7.
25 Fukuen S, Fukuda T, Maune H *et al.* Novel detection assay by PCR-RFLP and frequency of the CYP3A5 SNPs, CYP3A5*3 and *6, in a Japanese population. *Pharmacogenetics* 2002;**12:**331–4.
26 Mathijssen RH, Marsh S, Karlsson MO *et al.* Irinotecan pathway genotype analysis to predict pharmacokinetics. *Clin Cancer Res* 2003;**9:**3246–53.
27 Kim RB, Leake BF, Choo EF *et al.* Identification of functionally variant MDR1 alleles among European Americans and African Americans. *Clin Pharmacol Ther* 2001;**70:**189–99.
28 Hoffmeyer S, Burk O, von Richter O *et al.* Functional polymorphisms of the human multidrug-resistance gene: multiple sequence variations and correlation of one allele with P-glycoprotein expression and activity in vivo. *Proc Natl Acad Sci U S A* 2000; **97:**3473–8.
29 Nakajima M, Fujiki Y, Kyo S *et al.* Pharmacokinetics of paclitaxel in ovarian cancer patients and genetic polymorphisms of CYP2C8, CYP3A4, and MDR1. *J Clin Pharmacol* 2005;**45:**674–82.
30 Penson RT, Oliva E, Skates SJ *et al.* Expression of multidrug resistance-1 protein inversely correlates with paclitaxel response and survival in ovarian cancer patients: a study in serial samples. *Gynecol Oncol* 2004;**93:**98–106.

Accepted for publication December 14, 2005

O-[^{18}F]fluoromethyl-L-tyrosine is a potential tracer for monitoring tumour response to chemotherapy using PET: an initial comparative in vivo study with deoxyglucose and thymidine

Gengo Yamaura[1], Takashi Yoshioka[1], Hiroshi Fukuda[2], Keichiro Yamaguchi[3], Manami Suzuki[3], Shozo Furumoto[4], Ren Iwata[4], Chikashi Ishioka[1]

[1] Department of Clinical Oncology, Institute of Development, Aging and Cancer, Tohoku University, 4-1 Seiryo-machi, Aoba ward, Sendai 980-8575, Japan
[2] Department of Nuclear Medicine and Radiology, Institute of Development, Aging and Cancer, Tohoku University, Sendai, Japan
[3] Division of Nuclear Medicine, CYRIC, Tohoku University, Sendai, Japan
[4] Division of Radiopharmaceutical Chemistry, CYRIC, Tohoku University, Sendai, Japan

Received: 13 August 2005 / Accepted: 9 March 2006 / Published online: 9 June 2006

Abstract. *Purpose:* To compare the utility of a new artificial amino acid, *O*-[^{18}F]fluoromethyl-L-tyrosine ([^{18}F]FMT), for monitoring cancer chemotherapy with deoxyglucose and thymidine.
Methods: [^{18}F]FMT, [^{14}C]deoxyglucose ([^{14}C]DG) and [6-^{3}H]thymidine ([^{3}H]Thd) were applied in this study. A 2.5 mg/kg dose of mitomycin (MMC) was administered to AH272 rat hepatoma-bearing Donryu rats. Tumour uptake of each tracer was measured just before (baseline) and on days 1, 3, 5 and 7 after the MMC administration, 1 h after a mixture of [^{18}F]FMT, [^{14}C]DG and [^{3}H]Thd had been injected, and was shown as DURs (% injected dose/gram tissue normalised for the rat body weight). Dual-tracer macroautoradiographs with [^{18}F]FMT and [^{14}C]DG were also prepared.
Results: The tumour uptake for each tracer decreased earlier than did the tumour size. DURs (mean±SD) at baseline and on days 1, 3, 5 and 7 were as follows: [^{18}F]FMT: 4.68±0.72, 3.34±0.66, 3.13±0.72, 3.42±0.45, 3.01±0.32; [^{14}C]DG: 3.26±0.40, 3.09±0.55, 3.01±0.97, 2.28±0.35, 1.70±0.72; and [^{3}H]Thd: 2.23±0.46, 1.54±0.45, 1.28±0.37, 1.35±0.20, 0.94±0.12. Decrease in [^{18}F]FMT uptake compared with baseline was significant from day 1 ($p<0.01$), and the decrease in [^{3}H]Thd uptake was also significant on day 1 ($p<0.05$) and days 3–7 ($p<0.01$). However, decrease in [^{14}C]DG uptake was only significant from day 5 ($p<0.01$). Macroautoradiography suggested that the influence of inflammatory cells on the accumulation of [^{18}F]FMT in tumours is smaller than that on the accumulation of [^{14}C]DG.
Conclusion: [^{18}F]FMT uptake shows a rapid and sensitive response to chemotherapy, comparable to that of [^{3}H]Thd, suggesting that it may be applied as a powerful tracer for monitoring of proliferative activity after cancer chemotherapy using PET.

Keywords: *O*-[^{18}F]fluoromethyl-L-tyrosine – [^{18}F]fluorodeoxyglucose – [^{3}H]thymidine – PET – Cancer chemotherapy

Eur J Nucl Med Mol Imaging (2006) 33:1134–1139
DOI 10.1007/s00259-006-0126-2

Takashi Yoshioka (✉)
Department of Clinical Oncology, Institute of Development, Aging and Cancer, Tohoku University,
4-1 Seiryo-machi, Aoba ward,
Sendai 980-8575, Japan
e-mail: ytakashi@idac.tohoku.ac.jp
Tel.: +81-22-7178547, Fax: +81-22-7178548

Introduction

During the past decade, advances in positron emission tomography (PET) have facilitated the acquisition of information on metabolism in neoplasms to such an extent that it has become an essential tool in the management of cancer patients. The glucose analogue ^{18}F-fluoro-2-deoxy-D-glucose ([^{18}F]FDG) is the most frequently used tracer in PET studies in oncology, its application being based on increased glucose uptake in tumour cells owing to increased glycolysis [1]. [^{18}F]FDG PET has been successfully used to image various kinds of malignant tumour, for staging and restaging [2], and for monitoring the efficacy of cancer treatment [3–7]. However, [^{18}F]FDG is well known to exhibit non-specific uptake in inflammatory cells and granulation tissue [8], and this is a disadvantage in monitoring the results of therapy.

Increased amino acid metabolism is also a well-known characteristic of malignant tumours [9], both amino acid

transport and protein synthesis rates being enhanced in malignancies. Therefore, clinical interest in imaging protein metabolism with the aid of radiolabelled amino acids is expected to increase [10]. L-[*S*-methyl-^{11}C] methionine ([^{11}C]Met) is one of the most widely used agents for this purpose because of its simple labelling procedure [11] and high uptake in a number of tumours [12–16]. However, ^{18}F-fluorinated amino acids may have practical benefits for tumour diagnosis in PET studies, because the half-life of ^{18}F (109 min) is more suitable for whole-body tumour imaging than that of ^{11}C (20 min) [17].

^{18}F-labelled amino acids that enter the protein synthesis pathway, such as 2-[^{18}F]fluoro-L-tyrosine ([^{18}F]TYR) [18], have been developed as protein synthesis tracers but suffer from the disadvantage of also reflecting the maintenance of cells and not only cell proliferation [10, 19]. More recently, ^{18}F-labelled artificial amino acids, such as *O*-[^{18}F]fluoroethyl-L-tyrosine ([^{18}F]FET) [20] and [^{18}F]fluorine-α-methyl-tyrosine [21], have been developed, and these are amino acid transport tracers that are thought to be more directly related to cell proliferation [10]. In contrast to glucose, amino acids play only a minor role in the metabolism of inflammatory cells [22], so they might be expected to serve as more specific tracers for monitoring cancer treatment, especially chemotherapy, than [^{18}F]FDG. Since there have been no experimental in vivo studies to compare the utility of different radioactive tracers for monitoring chemotherapeutic effects, the present comparative investigation was performed.

O-[^{18}F]fluoromethyl-L-tyrosine ([^{18}F]FMT) is an amino acid transport tracer, developed in our institute [23, 24], which features ease of synthesis and a satisfactorily high radiochemical yield. In the present study, it was compared with glucose and nucleic acid metabolic tracers, using mitomycin chemotherapy of the AH272 rat hepatoma transplanted into Donryu rats as a suitable model.

Materials and methods

Radiopharmaceuticals

[^{18}F]FMT was synthesised according to the method of Iwata et al. with a radiochemical purity higher than 98% [23]. Briefly, [^{18}F] fluoromethyl triflate was bubbled through a dimethylsulphoxide solution of L-tyrosine disodium salt at room temperature, and the reaction mixture was purified by high-performance liquid chromatography (HPLC). 2-Deoxy-D-[1-^{14}C]glucose ([^{14}C]DG, specific activity 2.07 GBq/mmol, radiochemical purity 98.3%, Amersham Biosciences UK Limited) as a substitute for [^{18}F]FDG and [6-^{3}H] thymidine ([^{3}H]Thd, specific activity 814 GBq/mmol, radiochemical purity 99.8%, Amersham Biosciences UK Limited) were obtained commercially.

Animals, tumours and chemotherapy

Five-week-old male Donryu rats were injected subcutaneously under their back skin with a 0.1 ml suspension containing 3.0×10^6 AH272 cells. Chemotherapy was performed with commercially available mitomycin C (MMC, Kyowa Hakko Kogyo Co. Ltd.) on the 10th day after the inoculation, when the tumours had grown to between 1.0 and 1.5 cm in diameter. Rats were anaesthetised with the inhalation of ether, and 2.5 mg/kg of MMC dissolved in 0.2–0.4 ml of physiological saline was administered to each rat via a lateral tail vein.

Tumour growth study

Six rats per group were used for control and chemotherapy groups. Tumours were measured (length and width) with sliding calipers by the same person every day after the start of the experiment. The tumour volume (V) in mm^3 was calculated from the linear measurements using the formula: tumour volume (mm^3)=4×pi×((length (mm) plus width (mm))/2)^3/3. The relative mean tumour volume (RV) was calculated as V_i/V_o, where V_i is the mean tumour volume of a group at any given time and V_o is the mean tumour volume at the initial treatment. Growth curves after treatment were generated from the calculated RV.

Triple-tracer tissue distribution study

The triple-tracer tissue distribution studies were performed on four groups of six rats at 1, 3, 5 and 7 days after chemotherapy, and also on a control group of seven rats. After 8 h of fasting, a mixture of three tracers, consisting of 1.85 MBq [^{18}F]FMT, 74 kBq [^{14}C]DG and 74 kBq [^{3}H]Thd, in 0.2 ml of physiological saline, was injected via a lateral tail vein. Rats anaesthetised with ether were killed by decapitation 60 min after the injection and the tumours were removed and blotted. A cross-section of each tumour at its maximum diameter was sampled and weighed, followed by ^{18}F measurement with an automated NaI well counter (United Technologies Packard Auto-Gamma 500/800). Seven days later, when ^{18}F had decayed, tissue samples were prepared for liquid scintillation counting of ^{14}C and ^{3}H. Each sample was digested and bleached with 2 ml tissue solvent, Soluene-350 (PerkinElmer Life Sciences), in a heater at 50°C for 4–5 h. The samples were then mixed with 10 ml scintillation cocktail and left at room temperature overnight. The contamination of ^{3}H with ^{14}C was 1.3%, and that of ^{14}C with ^{3}H was 0.35%. Tissue radioactivity data were expressed as the differential uptake ratio (DUR): DUR = (tissue counts/tissue weight) / (injected dose counts/animal body weight).

The relative tumour uptake ratio was also calculated as DUR_i/DUR_o, where DUR_i is the mean DUR of a group at any given time and DUR_o is the mean DUR at the initial treatment.

Dual-tracer macroautoradiography

A control rat and another rat at 3 days after chemotherapy were prepared for dual-tracer macroautoradiography. After fasting overnight, a mixture of 37 MBq [^{18}F]FMT and 185 kBq [^{14}C]DG in 0.2 ml of physiological saline was injected via a lateral vein, and the rats were anaesthetised with ether and killed by decapitation 60 min thereafter. The tumours were quickly dissected, embedded in O.C.T. compound (Sakura Finetek Japan Co. Ltd.) and deep frozen in a block of dry ice. Several 20-μm-thick sections were cut and mounted on clean glass slides in a cryostat (HM-500 Carl Zeiss) at −20°C, air-dried and placed in direct contact with macroautoradiography films for 1.5 h to produce [^{18}F]FMT images. One week later, following the decay of ^{18}F, the same sections were placed in contact with separate films for 10 days to produce [^{14}C]DG images.

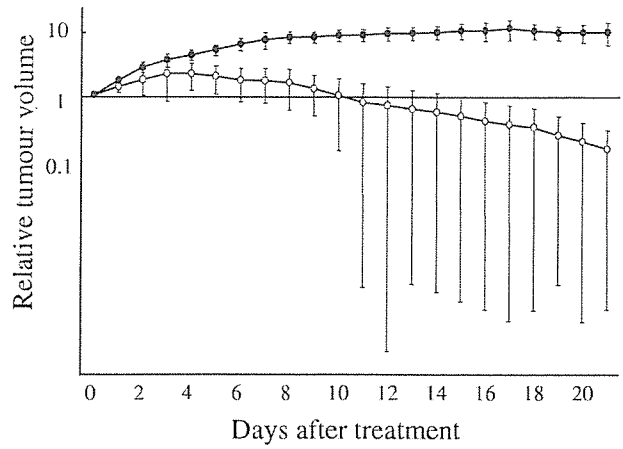

Fig. 1. The tumour growth curves for the chemotherapy (○) and control (●) groups. *Symbols* are mean values and *bars* are standard deviations. There were six rats in each group. In the control group, the tumours grew until day 18. In the chemotherapy group, tumour volumes begin to decrease on day 6, and the reductions were significant on day 11, as compared with the initial volume ($p<0.05$)

Microscopic examination

For comparison with the findings of dual-tracer macroautoradiography, a control rat and another rat at day 3 after chemotherapy were prepared for microscopic examination. Tumours were dissected, fixed with 10% neutral formalin and embedded in paraffin. Cross-sections with a thickness of 3 μm were produced with a microtome and stained with haematoxylin and eosin; the stained samples were examined with a BX51N microscope (Olympus) by the pathologist.

Statistical comparison

Student's *t* test was employed to determine the statistical significance of differences between tumour volumes and uptake data.

Ethics

The experimental protocol was approved by the Laboratory Animal Care Committee of Tohoku University.

Results

The growth curves for the chemotherapy and control groups are shown in Fig. 1. Each curve gives the mean and standard deviation for the relative tumour volume. In the control group, the volume increased until day 18. In the chemotherapy group, the relative tumour volumes slowed down from days 1 to 5, and began to decrease on day 6. The reduction became significant on day 11 (RV=0.75±0.76) as compared with the initial volume ($p<0.01$).

Data for the tumour uptake of [^{18}F]FMT, [^{14}C]DG and [^{3}H]Thd on the day before chemotherapy and on days 1, 3, 5 and 7 after chemotherapy are shown in Table 1, and the relative tumour uptake ratio curves of each tracer in Fig. 2. Decreases in uptake of all tracers were faster than those in the relative tumour volumes. The reduction in [^{18}F]FMT uptake compared with uptake on the day before chemotherapy was significant from day 1 ($p<0.01$), and [^{3}H]Thd uptake was also significantly reduced on day 1 ($p<0.05$) and days 3–7 ($p<0.01$). However, the decrease in [^{14}C]DG uptake occurred much later and was only significant from day 5 ($p<0.01$). The decreases in [^{14}C]DG and [^{3}H]Thd uptake after chemotherapy were larger than that in [^{18}F]FMT uptake. On the last day of the measurement, [^{14}C]DG and [^{3}H]Thd uptake had decreased to half of the untreated level, while [^{18}F]FMT uptake had decreased by one-third.

Macroautoradiographs of [^{18}F]FMT and [^{14}C]DG, and photographs of cross-sections of samples before and after chemotherapy are shown in Fig. 3. Tumour necrosis had been evident after chemotherapy, as shown in the photographs. Macroautoradiography of [^{18}F]FMT showed a diffuse pattern of uptake in tumour tissue, with gradual reduction of uptake in the necrotic area. On the other hand, [^{14}C]DG uptake was slightly spotty but dense close to the rim of the tumour, and there was strong contrast between the tumour and the necrotic area.

Microscopic examination was carried out separately from autoradiography at 3 days after chemotherapy, and the result is shown in Fig. 4. A large number of inflammatory cells appeared immediately adjacent to areas of necrosis.

Discussion

The present study provided clear evidence that uptake of [^{18}F]FMT and [^{3}H]Thd after MMC treatment of the AH272

Table 1. Tumour uptake of [^{18}F]FMT, [^{14}C]DG and [^{3}H]Thd after chemotherapy

	Pretreatment (control)	Day 1	Day 3	Day 5	Day 7
[^{18}F]FMT	4.68±0.72	3.34±0.66**	3.13±0.72**	3.42±0.45**	3.01±0.32**
[^{14}C]DG	3.26±0.40	3.09±0.55	3.01±0.97	2.28±0.35**	1.70±0.72**
[^{3}H]Thd	2.23±0.46	1.54±0.45*	1.28±0.37**	1.35±0.20**	0.94±0.12

Values are expressed as mean±standard deviation of DURs
The number of rats in each group was seven
DURs of each day after chemotherapy are compared with the DUR of the control
Statistical comparison: *$p<0.05$, **$p<0.01$ (Student's *t* test)

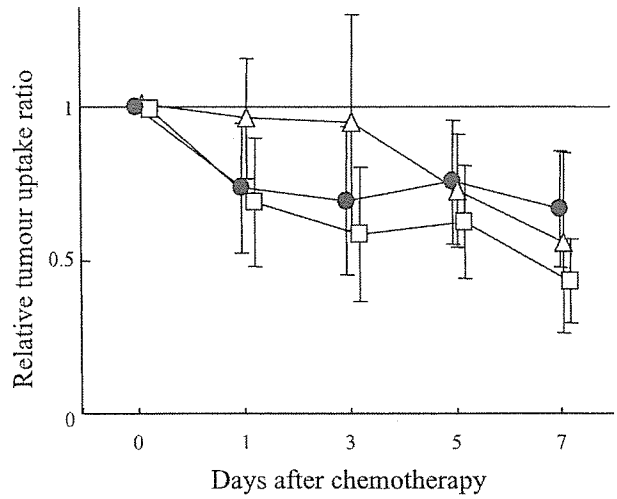

Fig. 2. Relative tumour uptake ratio curves of [^{18}F]FMT, [^{14}C]DG and [^{3}H]Thd after chemotherapy. *Symbols* are mean values and *bars* are standard deviations. ●, [^{18}F]FMT; △, [^{14}C]DG; □, [^{3}H]Thd

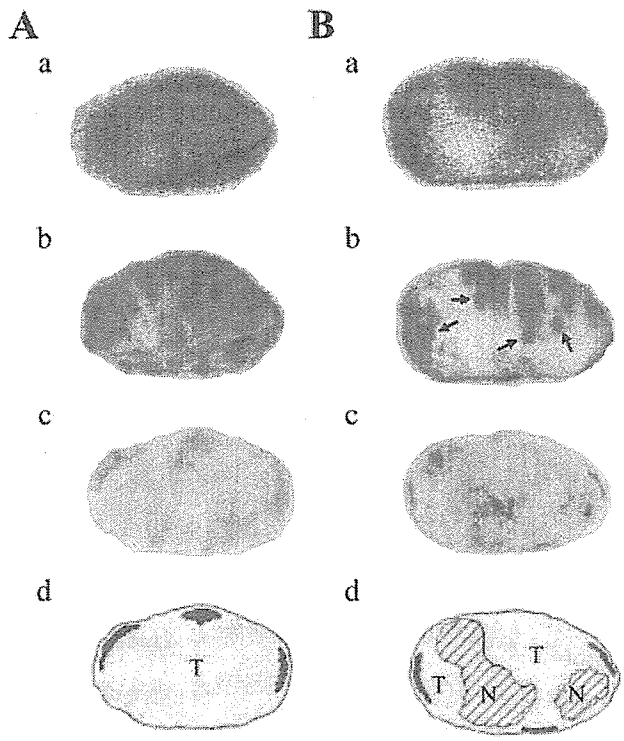

Fig. 3. Macroautoradiographs of control and MMC-treated tumours with [^{18}F]FMT and [^{14}C]DG, together with photographs and illustrations of their cross-sections. **A** is a control tumour and **B** is a tumour at 3 days after chemotherapy. **a** Macroautoradiographs of [^{18}F]FMT; **b** macroradioautographs of [^{14}C]DG; **c** photographs of the sample cross-sections; **d** illustrations of the photographs. In the illustrations, *T* indicates viable tumour and *N* indicates necrotic areas. The *arrow* in **B, b** indicates the rim of the tumour, where there is strong contrast between the tumour and the necrotic area on macroautoradiography with [^{14}C]DG

rat hepatoma transplanted into Donryu rats is more rapidly reduced than the uptake of [^{14}C]DG, providing an effective means for determination of early response to chemotherapy in vivo.

Amino acid transport tracers are amino acids that are only transported into the cells and do not actually participate in protein synthesis [10], examples being [^{18}F]FMT [23, 24], [^{18}F]FET [20] and [^{18}F]fluorine-α-methyl-tyrosine [21]. [^{11}C]Met is the most widely used amino acid tracer, and shows a well-documented rapid response to cancer radiotherapy [25]. However, clinical use is limited by high accumulation in the normal liver, pancreas and small intestine, and clinical interpretation of change in uptake of [^{11}C]Met during treatment is difficult because it participates in too many metabolic pathways [19]. The other amino acid tracers that enter protein synthesis, such as [^{18}F]TYR, are unsuitable for the evaluation of cell proliferation since protein synthesis is not always related to cell proliferation, in that the protein may be used for maintenance of cells [10]. Imaging with amino acid transport tracers shows the sum of protein synthesis and non-protein synthesis processes and the total amino acid signal is likely to correlate with the cell proliferation; thus these tracers are thought to be more appropriate for monitoring of chemotherapy. The fact that [^{18}F]FMT and [^{3}H]Thd, used as a nucleic acid tracer, showed similar changes in the time course after chemotherapy is of clear interest in this respect.

As already mentioned, in the present study, macro-autoradiography demonstrated [^{18}F]FMT to be diffusely distributed in tumour tissue with gradual reduction of uptake in the necrotic area, while [^{14}C]DG uptake was slightly spotty but dense close to the rim of the tumour, with marked contrast between the tumour and the necrotic area. Microscopy showed many inflammatory cells between the tumour and the necrotic area. Rau et al. [26]

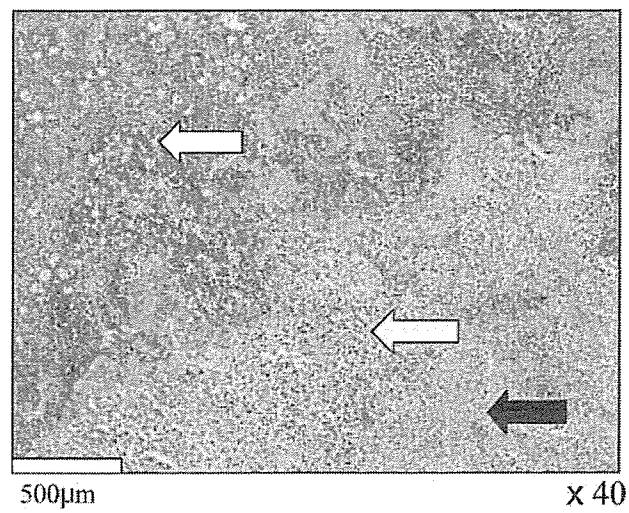

Fig. 4. Microscopic examination of tumour at day 3 after chemotherapy. The *white, yellow and black arrows* indicate the viable tumour, inflammatory cells and necrotic areas, respectively. A number of inflammatory cells appear around the necrotic area

and Suzuki et al. [27] respectively reported [^{18}F]FET and [^{18}F]FMT to show only limited accumulation in acute and chronic inflammatory lesions, whereas there is evidence that [^{18}F]FDG is readily taken up by inflammatory cells and granulation tissue [8]. However, it has also been reported that prenecrotic or hypoxic cells [28] and apoptosis [29] can be responsible for high accumulation of [^{18}F]FDG, and it might be difficult to explain the dense accumulation of [^{14}C]DG in the rim of the tumour only by reference to the presence of inflammatory cells. Nevertheless, at least in our study, it is possible that inflammatory cells affected the accumulation of [^{14}C]DG but not [^{18}F]FMT, and thus [^{18}F]FMT might be more appropriate than [^{18}F]FDG for the early detection of chemotherapeutic effects.

In our study, the final range of decrease in [^{18}F]FMT uptake after chemotherapy tended to be small, compared with the decrease in [^{14}C]DG uptake, in line with earlier findings for [^{14}C]Met after radiotherapy in comparison with [^{18}F]FDG [3]. Amino acids are also used for non-protein synthesis and this might be at least partially responsible for the small reduction in [^{18}F]FMT uptake after chemotherapy, but actual causes remain to be clarified. The small reduction in the amino acid transport tracers after chemotherapy or radiotherapy might be a disadvantage when using them to evaluate the effect of treatment.

We employed [^{18}F]FMT as an amino acid transport tracer in this study since it was recently developed in our institute using [^{18}F]fluoromethyl triflate as a novel [^{18}F]fluoromethylating agent [30]. The preparation method is simpler and more efficient than that for [^{18}F]FET and [^{18}F]fluorine-α-methyl-tyrosine, and is suitable for routine production [23] of sufficient amounts for a number of patients and distribution to satellite PET centres.

Recent development of 3′-deoxy-3′-[^{18}F]fluoro-thymidine ([^{18}F]FLT) has made it possible to obtain DNA synthesis-specific proliferative images of tumours [31, 32], and [^{18}F]FLT has been expected to be applicable for the monitoring of antiproliferative therapy [33]. In our study, the reduction in the uptake of [^{3}H]Thd was similar to that in [^{18}F]FMT, suggesting that in this model [^{18}F]FLT would perform as well as [^{18}F]FMT. Because [^{18}F]FLT reflects DNA synthesis, it might be more specific for monitoring antiproliferative therapy than amino acid transport tracers. However, because amino acid transport tracers reflect the sum of protein synthesis and non-protein synthesis processes, they could yield some information beyond that on DNA synthesis. Further comparative studies on the particular advantages and disadvantages of [^{18}F]FMT and amino acid transport tracers will be needed.

To our knowledge, this study is the first experimental in vivo study to compare the utility of an amino acid transport tracer and a glucose analogue for monitoring of chemotherapeutic effects. Recently, Pauleit et al. reported [^{18}F]FET to be inferior to [^{18}F]FDG as a PET tracer for general tumour diagnosis [34], but our data suggest that amino acid transport tracers may be superior for assessing treatment efficacy.

In conclusion, [^{18}F]FMT showed as rapid and sensitive a response to chemotherapy as [^{3}H]Thd, with advantages over [^{14}C]DG. The data suggest that [^{18}F]FMT is a promising PET tracer for monitoring proliferative activity after cancer chemotherapy and that clinical trials should now be considered.

Acknowledgements. This work was supported by Grants-in-Aid for Scientific Research (No. 13670910) from the Ministry of Education, Science, Sports, Culture and Technology, and for Cancer Research (11S-3) from the Ministry of Health, Labor, and Welfare, Japan.

References

1. Warburg O. On the origin of cancer cells. Science 1956;123:309–14
2. Gambhir SS, Czernin J, Schwimmer J, Silverman DH, Coleman RE, Phelps ME. A tabulated summary of the FDG PET literature. J Nucl Med 2001;42:1S–93S
3. Kubota K, Ishiwata K, Kubota R, Yamada S, Tada M, Sato T, et al. Tracer feasibility for monitoring tumor radiotherapy: a quadruple tracer study with fluorine-18-fluorodeoxyglucose or fluorine-18- fluorodeoxyuridine, L-[methyl-^{14}C]methionine, [6-^{3}H]thymidine, and gallium-67. J Nucl Med 1991;32: 2118–23
4. Yoshioka T, Takahashi H, Oikawa H, Maeda S, Ido T, Akaizawa T, et al. Influence of chemotherapy on FDG uptake by human cancer xenografts in nude mice. J Nucl Med 1997;38:714–7
5. Kostakoglu L, Goldsmith SJ. ^{18}F-FDG PET evaluation of the response to therapy for lymphoma and for breast, lung, and colorectal carcinoma. J Nucl Med 2003;44:224–39
6. Kostakoglu L, Goldsmith SJ. PET in the assessment of therapy response in patients with carcinoma of the head and neck and of the esophagus. J Nucl Med 2004;45:56–68
7. Weber WA. Use of PET for monitoring cancer therapy and for predicting outcome. J Nucl Med 2005;46:983–95
8. Kubota R, Kubota K, Yamada S, Tada M, Ido T, Tamahashi N. Microautoradiographic study for the differentiation of intratumoral macrophages, granulation tissues and cancer cells by the dynamics of fluorine-18-fluorodeoxyglucose uptake. J Nucl Med 1994;35:104–12
9. Weber G. Biochemical strategy of cancer cells and the design of chemotherapy: G. H. A. Clowes Memorial Lecture. Cancer Res 1983;43:3466–92
10. Jager PL, Vaalburg W, Pruim J, de Vries EG, Langen KJ, Piers DA. Radiolabeled amino acids: basic aspects and clinical applications in oncology. J Nucl Med 2001;42:432–45
11. Langstrom B, Antoni G, Gullberg P, Halldin C, Malmborg P, Nagren K, et al. Synthesis of L- and D-[methyl-^{11}C]methionine. J Nucl Med 1987;28:1037–40
12. Kubota K, Matsuzawa T, Ito M, Ito K, Fujiwara T, Abe Y, et al. Lung tumor imaging by positron emission tomography using C-11 L-methionine. J Nucl Med 1985;26:37–42
13. Leskinen-Kallio S, Lindholm P, Lapela M, Joensuu H, Nordman E. Imaging of head and neck tumors with positron emission tomography and [^{11}C]methionine. Int J Radiat Oncol Biol Phys 1994;30:1195–9
14. Lindholm P, Leskinen S, Nagren K, Lehikoinen P, Ruotsalainen U, Teras M, et al. Carbon-11-methionine PET imaging of malignant melanoma. J Nucl Med 1995;36:1806–10

15. Jansson T, Westlin JE, Ahlstrom H, Lilja A, Langstrom B, Bergh J. Positron emission tomography studies in patients with locally advanced and/or metastatic breast cancer: a method for early therapy evaluation? J Clin Oncol 1995;13:1470–7
16. Sato N, Suzuki M, Kuwata N, Kuroda K, Wada T, Beppu T, et al. Evaluation of the malignancy of glioma using ^{11}C-methionine positron emission tomography and proliferating cell nuclear antigen staining. Neurosurg Rev 1999;22:210–4
17. Laverman P, Boerman OC, Corstens FH, Oyen WJ. Fluorinated amino acids for tumour imaging with positron emission tomography. Eur J Nucl Med Mol Imaging 2002;29:681–90
18. Coenen HH, Kling P, Stocklin G. Cerebral metabolism of L-[2-^{18}F]fluorotyrosine, a new PET tracer of protein synthesis. J Nucl Med 1989;30:1367–72
19. Ishiwata K, Enomoto K, Sasaki T, Elsinga PH, Senda M, Okazumi S, et al. A feasibility study on L-[1-carbon-11]tyrosine and L-[methyl-carbon-11]methionine to assess liver protein synthesis by PET. J Nucl Med 1996;37:279–85
20. Wester HJ, Herz M, Weber W, Heiss P, Senekowitsch-Schmidtke R, Schwaiger M, et al. Synthesis and radiopharmacology of *O*-(2-[^{18}F]fluoroethyl)-L-tyrosine for tumor imaging. J Nucl Med 1999;40:205–12
21. Inoue T, Tomiyoshi K, Higuichi T, Ahmed K, Sarwar M, Aoyagi K, et al. Biodistribution studies on L-3-[fluorine-18] fluoro-alpha-methyl tyrosine: a potential tumor-detecting agent. J Nucl Med 1998;39:663–67
22. Kubota K, Matsuzawa T, Fujiwara T, Sato T, Tada M, Ido T, et al. Differential diagnosis of AH109A tumor and inflammation by radioscintigraphy with L-[methyl-^{11}C]methionine. Jpn J Cancer Res 1989;80:778–82
23. Iwata R, Furumoto S, Pascali C, Bogni A, Ishiwata K. Radiosynthesis of *O*-[^{11}C]methyl-L-tyrosine and *O*-[^{18}F]fluoromethyl-L-tyrosine as potential PET tracers for imaging amino acid transport. J Label Compd Radiopharm 2003;46:555–66
24. Ishiwata K, Kawamura K, Wang WF, Furumoto S, Kubota K, Pascali C, et al. Evaluation of *O*-[^{11}C]methyl-L-tyrosine and *O*-[^{18}F]fluoromethyl-L-tyrosine as tumor imaging tracers by PET. Nucl Med Biol 2004;31:191–98
25. Kubota K, Matsuzawa T, Takahashi T, Fujiwara T, Kinomura S, Ido T, et al. Rapid and sensitive response of carbon-11-L-methionine tumor uptake to irradiation. J Nucl Med 1989; 30:2012–016
26. Rau FC, Weber WA, Wester HJ, Herz M, Becker I, Kruger A, et al. *O*-(2-[^{18}F]fluoroethyl)-L-tyrosine (FET): a tracer for differentiation of tumour from inflammation in murine lymph nodes. Eur J Nucl Med Mol Imaging 2002;29:1039–46
27. Suzuki M, Yamaguchi K, Honda G, Iwata R, Furumoto S, Jeong MG, et al. An experimental study on *O*-[^{18}F]fluoromethyl-L-tyrosine for differentiation between tumor and inflammatory tissues. Ann Nucl Med 2005;19:589–95
28. Kubota R, Kubota K, Yamada S, Tada M, Ido T, Tamahashi N. Active and passive mechanisms of [fluorine-18] fluorodeoxyglucose uptake by proliferating and prenecrotic cancer cells in vivo: a microautoradiographic study. J Nucl Med 1994; 35:1067–75
29. Haberkorn U, Bellemann ME, Brix G, Kamencic H, Morr I, Traut U, et al. Apoptosis and changes in glucose transport early after treatment of Morris hepatoma with gemcitabine. Eur J Nucl Med 2001;28:418–25
30. Iwata R, Pascali C, Bogni A, Furumoto S, Terasaki K, Yanai K. [^{18}F]fluoromethyl triflate, a novel and reactive [^{18}F]fluoromethylating agent: preparation and application to the on-column preparation of [^{18}F]fluorocholine. Appl Radiat Isot 2002;57:347–52
31. Shields AF, Grierson JR, Dohmen BM, Machulla HJ, Stayanoff JC, Lawhorn-Crews JM, et al. Imaging proliferation in vivo with [F-18]FLT and positron emission tomography. Nat Med 1998;4:1334–336
32. Buck AK, Halter G, Schirrmeister H, Kotzerke J, Wurziger I, Glatting G, et al. Imaging proliferation in lung tumors with PET: ^{18}F-FLT versus ^{18}F-FDG. J Nucl Med 2003;44:1426–31
33. Waldherr C, Mellinghoff IK, Tran C, Halpern BS, Rozengurt N, Safaei A, et al. Monitoring antiproliferative responses to kinase inhibitor therapy in mice with 3′-deoxy-3′-^{18}F-fluorothymidine PET. J Nucl Med 2005;46:114–20
34. Pauleit D, Stoffels G, Schaden W, Hamacher K, Bauer D, Tellmann L, et al. PET with *O*-(2-^{18}F-fluoroethyl)-L-tyrosine in peripheral tumors: first clinical results. J Nucl Med 2005;46:411–6

British Journal of Cancer (2006) 94, 1586–1591

www.bjcancer.com

Clinical Studies

Clinical outcome and risk factors for recurrence in borderline ovarian tumours

Y Yokoyama*[,1], T Moriya[2], T Takano[3], T Shoji[4], O Takahashi[5], K Nakahara[6], H Yamada[7], N Yaegashi[3], K Okamura[3], T Izutsu[4], T Sugiyama[4], T Tanaka[5], H Kurachi[6], A Sato[7], T Tase[8] and H Mizunuma[1]

[1]Department of Obstetrics and Gynecology, Hirosaki University School of Medicine, 5 Zaifu-cho, Hirosaki 036-8562, Japan; [2]Department of Pathology, Tohoku University School of Medicine, 1-1 Seiryo-cho, Aoba-ku, Sendai 980-8574, Japan; [3]Department of Obstetrics and Gynecology, Tohoku University School of Medicine, 1-1 Seiryo-cho, Aoba-ku, Sendai 980-8574, Japan; [4]Department of Obstetrics and Gynecology, Iwate Medical University School of Medicine, 19-1 Uchimaru, Morioka 020-8505, Japan; [5]Department of Obstetrics and Gynecology, Akita University School of Medicine, 1-1-1 Hondo, Akita 010-8543, Japan; [6]Department of Obstetrics and Gynecology, Yamagata University School of Medicine, 2-2-2 Iidanishi, Yamagata 990-9585, Japan; [7]Department of Obstetrics and Gynecology, School of Medicine Fukushima Medical University, 1 Hikarigaoka, Fukushima 960-1295, Japan; [8]Department of Gynecology, Miyagi Cancer Center, 47-1 Aishima, Natori 981-1293, Japan

We investigated the long-term prognosis of borderline ovarian tumours and determined risk factors for recurrence. One hundred and twenty-one borderline ovarian tumours treated between 1994 and 2003 at the participating institutions in the Tohoku Gynecologic Cancer Unit were retrospectively investigated for clinical stage, histopathological subtype, surgical technique, postoperative chemotherapy, the presence or absence of recurrence, and prognosis. The median follow-up period was 57 months (1–126 months). One hundred and nine cases (90.6%) were at clinical stage I. The histopathological subtypes consisted of 91 cases of mucinous tumour (75.2%), 27 cases of serous tumour (22.3%), and three cases of endometrioid tumour. Conservative surgery was used in 53 cases (43.8%), radical surgery in 68 cases (56.2%), a staging laparotomy in 43 cases (35.5%), and postoperative adjuvant therapy in 30 cases (24.8%). Recurrence was found in eight cases, but no tumour-related deaths were reported. Although no significant difference in disease-free survival rate was seen between different clinical stages, the difference in disease-free survival rate between serous and nonserous (mucinous and endometrioid) types was significant ($P<0.05$). The 10-year disease-free survival rate was 89.1% for the radical surgery group and 57.4% for the conservative surgery group – this difference was significant ($P<0.05$). In the conservative surgery group, cystectomy and serous tumour were independent risk factors for recurrence. Although recurrence was observed, the long-term prognosis of borderline ovarian tumour was favourable, without tumour-related deaths. Considering the favourable prognosis, conservative surgery can be chosen as far as the patient has a nonserous tumour and receive adnexectomy. However, in cases of serous type and/or receiving cystectomy special care should be given as relative risk rates of recurrence elevate by 2–4-folds.

British Journal of Cancer (2006) **94,** 1586–1591. doi:10.1038/sj.bjc.6603139 www.bjcancer.com
Published online 9 May 2006

Keywords: borderline ovarian tumour; conservative surgery; cystectomy; serous tumour; multivariate analysis

Taylor (1929) found that some epithelial ovarian tumours showed clinically intermediate behaviour between benign and malignant, and called them 'semimalignant'. The International Federation of Gynecology and Obstetrics (FIGO) has formally introduced this concept as 'carcinoma of low malignant potential' in 1971, and the World Health Organization (WHO) as 'borderline tumour' in 1973, when the histological diagnostic criteria was proposed. The concept of borderline ovarian tumours was histologically defined as a disease entity that had been proposed clinically, and the adequacy of this histological definition has been repeatedly verified clinically.

*Correspondence: Dr Y Yokoyama;
E-mail: yokoyama@cc.hirosaki-u.ac.jp
Revised 13 February 2006; accepted 31 March 2006; published online 9 May 2006

With an accumulated experience and knowledge regarding the characteristics and management of borderline ovarian tumours, reclassification and redefinition have been attempted (Seidman and Kurman, 1996), and new prognostic factors have been proposed (de Nictolis *et al*, 1992; Gershenson *et al*, 1999). At present, many conflicting reports are causing confusion. As many of the patients are relatively young (Harris *et al*, 1992), preservation of fertility has been attempted with favourable results (Morice *et al*, 2001). However, there are also reports of recurrence or poor prognosis (Kaern *et al*, 1993; Gilks, 2003), and more precise prognostic factors are required. We believe that it is important to get a clear picture of the present status of borderline ovarian tumours, as it has been more than 30 years since the introduction of the concept of these tumours. Our retrospective multicentre study conducted an overall clinical analysis of borderline ovarian tumours. Our ultimate aim is to investigate the long-term prognosis of borderline ovarian tumours, and to determine the risk factors for recurrence.

MATERIALS AND METHODS

Information on 124 patients with a diagnosis of epithelial borderline ovarian tumour who were treated at the Tohoku Gynecologic Cancer Unit consisting of eight institutes from 1994 to 2003 was collected using each institutional databases.

Central pathological review was adopted in this study. One of the authors reviewed 124 cases diagnosed by the gynaecological pathologists of each institutes concerning histologic typing and grading of the primary lesion and 121 cases of those were determined as an epithelial borderline tumour. The histopathologic criteria embodied in a recent conference with published commentaries (Bell *et al*, 2004; Ronnett *et al*, 2004), some of which are included in the current WHO classification of ovarian tumours (Tavassoli and Devilee, 2003) were used for the diagnosis of borderline ovarian tumours in this study. These tumours were staged according to FIGO criteria (1987).

Radical surgery was defined as hysterectomy with bilateral salpingo-oophorectomy. Conservative surgery was defined as any surgery that preserved the uterus and one or both ovaries. Conservative surgical procedure was performed as cystectomy or adnexectomy. Peritoneal cytology was performed systematically in both surgical procedures. Surgical staging in the present study was defined as including peritoneal cytology, omentectomy, and pelvic lymphadenectomy with or without paraaortic exploration (lymphadenectomy or biopsy or palpation), and peritoneal biopsy in radical or conservative surgery on occasion. These surgical procedures were performed depending on the surgical teams who provided the treatment and whether borderline tumour was diagnosed during or after the surgical procedure.

With regard to adjuvant chemotherapy, all women with advanced disease, those with stage Ic, and those with a likely persistence of residual tumour after cystectomy received platinum-based treatment in the early years of this study. Thereafter, chemotherapy was usually confined to women with advanced disease.

Comparisons of categorical variables were conduced by two-tailed χ^2 and Fisher's exact tests where appropriate. Evaluation of independent factors predicting disease-specific recurrence was conducted by nominal logistic regression analysis. Survival estimates were calculated using the Kaplan–Meier product limit method. Comparison between survival curves was made using the generalised Wilcoxon's test. Statistical significance was set at $P<0.05$. The patients who lost to follow-up were censored from the survival data.

Detailed information regarding patient's characteristics, treatment method, recurrence, and prognosis of the disease was abstracted from the medical record. We did not request institutional review board approval for this study because of its retrospective nature.

RESULTS

The median age of patients was 43 years old (range 15–76 years). Fifty-one patients (42.1%) were below 40 years of age, and 29

Table 1 Clinical and histopathologic characteristics of patients with borderline tumours

	Alive with NED	Recurrence	Died of disease	Died of ICD	Lost	Total
Number of patients	94	8	0	2	17	121
Age (years)						
<20	7	0	0	0	0	7
20–30	14	1	0	0	4	19
31–40	19	4	0	0	2	25
41–50	14	1	0	0	2	17
51–60	17	1	0	1	5	24
> 60	23	1	0	1	4	29
Histological type						
Mucinous	73	4	0	2	12	91
Serous	19	4	0	0	4	27
Endometriod	2	0	0	0	1	3
Stage						
Ia	62	4	0	2	10	78
Ib	1	0	0	0	0	1
Ic	24	3	0	0	3	30
II	2	0	0	0	0	2
IIIa	0	1	0	0	1	2
IIIb	1	0	0	0	1	2
IIIc	3	0	0	0	1	4
IV	1	0	0	0	0	1
Unknown	0	0	0	0	1	1
Surgical procedure						
Radical	57	2	0	2	7	68
Conservative	37	6	0	0	10	53
Staging laparotomy						
Staged	36	3	0	1	3	43
Unstaged	58	5	0	1	14	78
Adjuvant chemotherapy						
Yes	22	4	0	1	3	30
No	72	4	0	1	14	91

NED = no evidence of disease; ICD = intercurrent disease.